

THE 2-D PLASMA THERMAL JET SIMULATIONS WITH SUBSTRATE INTERACTION

by

**Nouredine BOUCHEFFA^{a*}, Abdellah ABDELLAH ELHADJ^a,
and Redha REBHI^b**

^aLaboratoire de Mecanique Physique et Modelisation Mathematique,
University of Medea, Meda, Algeria

^bDepartment of Mechanical Engineering, Faculty of Technology, University of Medea,
Medea, Algeria

Original scientific paper
<https://doi.org/10.2298/TSCI190722212B>

This paper presents plasma thermal jet simulations with substrate interaction. In this work, 2-D plasma thermal jet simulations will be presented using the ANSYS-CFX code with taking into account the interaction fluid-substrate during thermal spraying. Two models of turbulence are used such as the shear stress transport $k-\omega$ (SST- $k-\omega$) and Re-normalization group (RNG- $k-\epsilon$). The governing parameters of the problem under study are the plasma gas power, the nozzle exit temperature and velocity profiles, the plasma jet temperature and velocity fields and the substrate temperature. The experimental and numerical results are presented in order to carry out a comparison between these results. Moreover, transient simulations will be also treated for different x-positions and different values of time. The distribution of temperature of the substrate will be also presented.

Key words: *plasma, thermal spray, substrate, SST- $k-\omega$, RNG- $k-\epsilon$, argon, ANSYS-CFX, 2-D jet*

Introduction

The modelling of plasma thermal spraying processes has experienced a great evolution in last year's due to the very rapid evolution of computers and to the progress made in the field of CFD codes. Modelling the spray process allows a better understanding of the process sequences during thermal spraying [1-3]. Many works have widely studied influence of the plasma thermal process parameters. Huang *et al.* [4] have studied plasma thermal spraying with two fluids model that the turbulent plasma jet is treated as a two-phase mixture. Chang-Zi *et al.* [5] worked on the plasma nitriding and Ti/TiN multilayer coating duplex treatment in order to increase the corrosion resistance of the commercial pure iron. Bolot *et al.* [6] have studied the use of a low Reynolds extension the Chen-Kim $k-\epsilon$ model to predict thermal exchanges in the case of an impinging argon/hydrogen plasma jet under atmospheric plasma spraying conditions. Qunbo *et al.* [7] model deals with the influence of operating parameters such as current, primary gas-flow and secondary gas-flow on the heat and state of acceleration of particles and on the final quality of the coating. They studied using the CFD code FLUENT, the typical process of an Ar-He plasma jet, by analyzing the influence of the current, the flow of Ar, as well as the flow of He on the temperature field and that of speed. Abdellah

* Corresponding author, e-mail: asphonour@gmail.com

El-hadj *et al.* [8] compared the two turbulence models $k-\varepsilon$ standard and RNG- $k-\varepsilon$ in a plasma spray discharging into the ambient air. It has been considered that the presence of the injected particles does not significantly affect the plasma. The authors used the finite volume method (FEM) using CFD Fluent Code. Selezneva and Bolos [9] studied numerically the flow of a plasma spraying downstream of a plasma torch, by means of a convergent-divergent nozzle adjustment. In this study, the authors attempted to construct a global supersonic plasma flow model and to make a comparative analysis with the subsonic one. Zhang *et al.* [10] used heat transfer theory, fluid mechanics and computational methods to simulate the temperature profile over the surface of an organic body or coating. The model identifies the critical parameters, such as scanning rate, flame power and polymer thickness, and predicts their influence on temperature profiles during impingement due to a moving flame. Murphy and Arundell [11] and Murphy [12] have calculated values of the viscosity, thermal conductivity, and electrical conductivity of Ar, Ni, and O plasmas and mixtures of Ar and Ni and O, are presented. Selvan *et al.* [13] have studied the effect of arc current, gas-flow rate, stand-off distance, type of substrate material and environment around the substrate on the thermal flux from the plasma to substrate and also the substrate temperature. Chen and Li [14] were interested in 3-D modelling of thermal plasma systems by calculating the characteristics of 3-D flow and heat flow. It is shown that when the particles in question and its gas carrier are injected into a plasma jet through a single port at the sidewall of the jet, the appreciable effects of 3-D and heat transfer flows appear and cannot be well described by 2-D models. These authors have studied the effects of the movement of particles and their heating in the plasma jet. The work of Qunbo *et al.* [15] consists of a model based on the calculation of the velocity, the temperature of the plasma jet and the Molar concentration fields of argon in a 3-D space. Important 3-D information, such as continuous isothermal lines, iso-velocity lines and the 3-D aspect of the plasma jet, were presented by these authors. This information will theoretically be more benefit for the analysis of the evolution of the temperature, the trajectory of the particles entrained, the state of melting of particles in the deposition of the coatings. In their study, Bolot *et al.* [16] worked on the case of an Ar-H plasma jet discharging into air, an impinging on a flat structure is considered and the results obtained for the energy flux transferred to the substrate are compared to those obtained from semi-empirical laws found in the literature and deduced from experimental measurements. Hugot *et al.* [17] have studied the thermal flux transferred from the plasma to the substrate. Their work has also treated the 2-D thermomechanical model developed with CAST3M CEA numerical code in order to determine the residual stress development during a zirconia coatings. The profiles of temperature and velocity have been widely studied and presented in several works. Gonzalez *et al.* [18] have predicted that with a lateral arc attachment condition, the temperature and velocity profiles at the nozzle exit are not symmetric [13-18]. Selvan *et al.* [19] explain in their works that the temperature and velocity profiles at the nozzle exit are simulated from the plasma arc model for a set of experimental conditions. Mariaux and Vardelle [20] have used an exponential formulas for velocity and temperature profiles. Otherwise, the time-dependent velocity and enthalpy profiles at the plasma torch exit resulting from the MHD calculations inside the torch nozzle have been used by Marchand *et al.* [21] as input data for the boundary conditions at nozzle exit.

The goal of this work is to simulate a 2-D thermal plasma jet by using the ANSYS-CFX code with two models of turbulence for different cases of effective powers. The velocity and temperature profiles at the inlet have been predicted and used as boundaries conditions. Transient simulations for plasma jet velocity and temperature fields and substrate temperature will be also presented.

Problem definition and mathematical formulation

In this paper the plasma jet is assumed steady, incompressible, subsonic in local thermo-dynamical equilibrium and turbulent. Moreover, is assumed that there is no segregation or chemical reactions in the gas phase. foregoing assumptions, a set of governing equations can be expressed in the simplified form:

$$\text{div}(\rho \bar{v} \phi) - \text{div}(\Gamma_\phi \text{grad} \phi) = S_\phi \tag{1}$$

where the dependent variable and property of, ϕ , diffusion coefficient, Γ_ϕ , and source term, S_ϕ , are presented in tab. 1.

Table 1. Equations in three dimensions for dependent variable/property, ϕ , diffusion coefficient, Γ_ϕ , and source term, S_ϕ

Equation	ϕ	Γ_ϕ	S_ϕ
Continuity	1	0	$\text{div}(\rho \bar{v})$
Momentum x	u	$\mu_{\text{eff}} = \mu + \mu_t$	$-\frac{\partial p}{\partial x} + \rho f_x + \text{div}\left(\mu_{\text{eff}} \frac{\partial \bar{v}}{\partial x}\right) + \frac{\partial}{\partial x}\left(-\frac{2}{3} \mu_{\text{eff}} \text{div} \bar{v}\right) - \frac{2}{3} \frac{\partial}{\partial x}(\rho k)$
Momentum y	v	μ_{eff}	$-\frac{\partial p}{\partial y} + \rho f_y + \text{div}\left(\mu_{\text{eff}} \frac{\partial \bar{v}}{\partial y}\right) + \frac{\partial}{\partial y}\left(-\frac{2}{3} \mu_{\text{eff}} \text{div} \bar{v}\right) - \frac{2}{3} \frac{\partial}{\partial y}(\rho k)$
Momentum z	w	μ_{eff}	$-\frac{\partial p}{\partial z} + \rho f_z + \text{div}\left(\mu_{\text{eff}} \frac{\partial \bar{v}}{\partial z}\right) + \frac{\partial}{\partial z}\left(-\frac{2}{3} \mu_{\text{eff}} \text{div} \bar{v}\right) - \frac{2}{3} \frac{\partial}{\partial z}(\rho k)$
Energy	h	$\rho(\lambda/c_p \rho) + \mu_t/\text{Pr}_t$	$S_H + \bar{v} \text{grad} p$
Mass fraction	y_i	$\rho D_i + \mu_t/\text{Sc}_t$	0

The S_H source term of the conservation equation of enthalpy, h , contains an additional term representing enthalpic diffusion. This term can be written:

$$S_H = \rho \sum_i D_i (h_i - h_k) \frac{\partial y_i}{\partial x_i} \tag{2}$$

where D_i is the diffusion coefficient of species i and ρ is the density. The equation of conservation of the mass of the species i is written:

$$\rho u_j \frac{\partial y_i}{\partial x_j} = \frac{\partial}{\partial x_j} \left(\rho D_i \frac{\partial y_i}{\partial x_j} \right) \tag{3}$$

Equation (4) summarizes different types of heat transfer wich exist in the plasma, where the term, $\bar{J}_{\text{elect}} \bar{E}$, is the joule effect energy supply:

$$\rho \bar{V} \text{grad} h = -\text{div}(\bar{q}_{\text{cond}}) - \text{div}(\bar{q}_{\text{ray}}) + \text{div}(\bar{\tau} \bar{V}) + \bar{J}_{\text{elect}} \bar{E} \tag{4}$$

The effective power supplied to the argon in order to generate the thermal plasma jet which leads to increase the enthalpy and the kinetic energy of the gas as shown by the following relation [1]:

$$P = \rho Q c_p (T_0 - T_a) + \frac{1}{2} \rho Q (U_0^2 - U_a^2) \tag{5}$$

where P , ρ , Q , c_p , T_0 , T_a , U_0 , and U_a are the power supplied to argon, density of argon at room temperature, argon flow at room temperature, the specific heat of argon, the average gas temperature at the outlet of the nozzle, the temperature of the gas at room temperature, the average speed of the plasma jet at the outlet of the nozzle, and the gas velocity at the outlet of the nozzle under the pressure, respectively, and temperature conditions of the laboratory.

Geometry and boundaries conditions

The geometry of the flow under consideration is shown in fig.1. The computational domain dimensions are 100 mm and 50 mm for length and height, respectively. The location of the inlet and outlet boundaries are shown in fig. 1, the nozzle exit diameter is 3.0 mm. For the case of 2-D simulation the x -axis aligned along the inlet flow and y -axis perpendicular to the x -axis.

The ANSYS CFX code, based on FVM, was used for the solution of the conservation equations that governing the problem (Navier-Stokes and turbulence quantities) for all of turbulence models used in this study [22]. Calculation are performed using the k - ε and k - ω variants models, *e.g.* RNG k - ε model and SST k - ω model [22]. The pre-processor *CFX* code associated with *Ansys* 16.0 is used for the construction of the computational domain and grid generation. A Cartesian structured grid non-uniform in the two direction X and Y is used. A special attention was paid to the generation, in particular near-wall treatment, because the grid adaptation it is a major step in validating the model for future analysis. The computation domain is divided into nine zones of non-uniform structured mesh as shown in figs. 1 and 2.

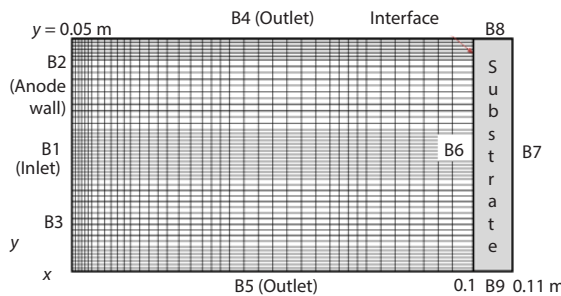


Figure 1. Schematic diagram

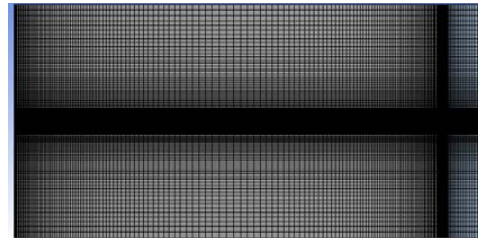


Figure 2. Computational domain (CFX meshing)

Moreover, tab. 2 presents the corresponding computational domain with 212910 calculation points and the corresponding types of boundaries conditions. Snabre *et al.* [1] use formulas derived from the enthalpy balance eq. (5) in order to carried out the values of T_{\max} and U_{\max} at the nozzle exit inlet. Where T_0 , U_0 , and U_a are calculated:

$$U_0 = \frac{U_a T_0}{T_a} \quad (6)$$

$$U_a = \frac{4Q}{\pi D^2} \quad (7)$$

$$T_0 = \frac{-b + \sqrt{(b^2 - 4ac)}}{2a} \quad (8)$$

with

$$a = \frac{1}{2} \rho Q \left(\frac{U_a}{T_a} \right)^2, \quad b = \rho Q c_p, \quad \text{and} \quad c = - \left(\frac{1}{2} \rho Q U_a^2 + \rho Q c_p T_a + P \right) \quad (9)$$

The comparison of the performance of two and 3-D models have been treated in the work of Gonzalez *et al.* [18] where the authors presented results which occur that the 2-D and 3-D temperature and velocity predictions are very close.

Table 2. The numbers of the nodes in the different zones of the mesh zones

Zone	Zone's name	Numbers of the nodes	Type of boundaries	
B1	Anode wall 1	60	Non-slip wall	$T = 500 \text{ K}$
B2	Anode wall 2	60	Non-slip wall	$T = 500 \text{ K}$
B3	Inlet (nozzle exit)	40	Temperature and velocity profiles	
B4	Outlet	150	Opening boundaries	
B5	Outlet	150	Opening boundaries	
B6	Interface	160	Conservative interface flux	
B7	Substrate (bottom Wall)	160	Heat transfer coefficient and outside temperature	Heat coefficient = $40 \text{ W/m}^2\text{K}$
B8	Substrate (side wall)	40	Non-slip wall	$T = 300 \text{ K}$
B9	Substrate (side wall)	40	Non-slip wall	$T = 300 \text{ K}$

By using eqs. (6)-(9) the results mentioned in tab. 3 can be carried out where Re is the Reynolds number.

Table 3. maximum values of temperatures and velocities for different cases and corresponding Reynolds number values

Cases	Power [W]	T_0 [K]	U_0 [ms^{-1}]	Re
Case a	790	661498	43672	473
Case b	1050	862517	56943	389
Case c	1300	1052870	6981	360
Case d	1780	1410734	93136	761

In the present model, the case of an argon plasma jet discharging into air was considered and properties of the argon plasma and the surrounding air were calculated separately assuming chemical equilibrium. The mixing of the plasma jet in the surrounding air was described using a mass fraction conservation equation [16]. The velocity and temperature profiles at the inlet (nozzle exit) of the model of this paper are taken from curves similar to the curves used by Gonzalez *et al.* [18] as shown in figs. 3(a) and 3(b). Also T_0 and U_0 mentioned in tab. 3 are considered as maximum values of these profiles for several cases.

The temperature dependent thermodynamic and transport properties of the plasma gases are taken from [11, 12, 23], these properties have been introduced to CFX-code by using functions and variables which have been specially defined.

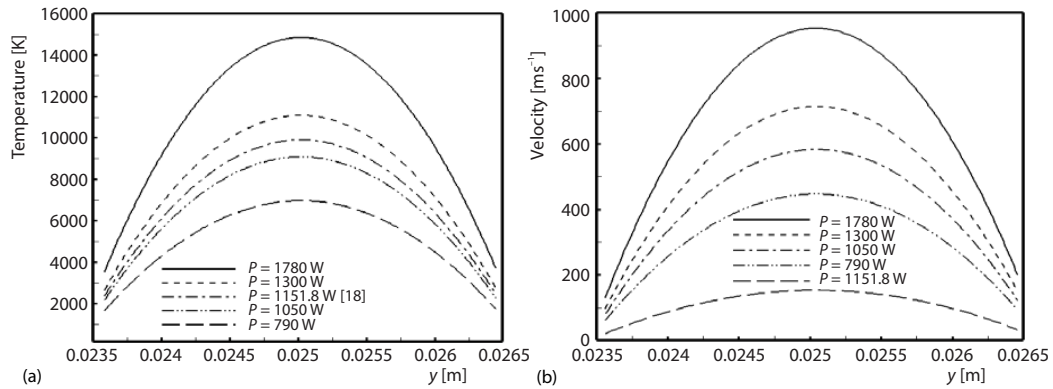


Figure 3. Temperature profiles at exit nozzle (a) and velocity profiles at exit nozzle (b)

Results and discussion

In this work, a 2-D case of a thermal plasma jet has been studied using argon as a plasma gas for different powers by using the ANSYS-CFX code. The computational domain dimensions for the plasma jet are 100 mm and 50 mm for length and height, respectively. The nozzle diameter is 3.0 mm, the argon flow rate is 8.4 Lpm, the x -axis is aligned along the inlet and the y -axis is perpendicular to the x -axis. Firstable, the results of a 2-D thermal plasma

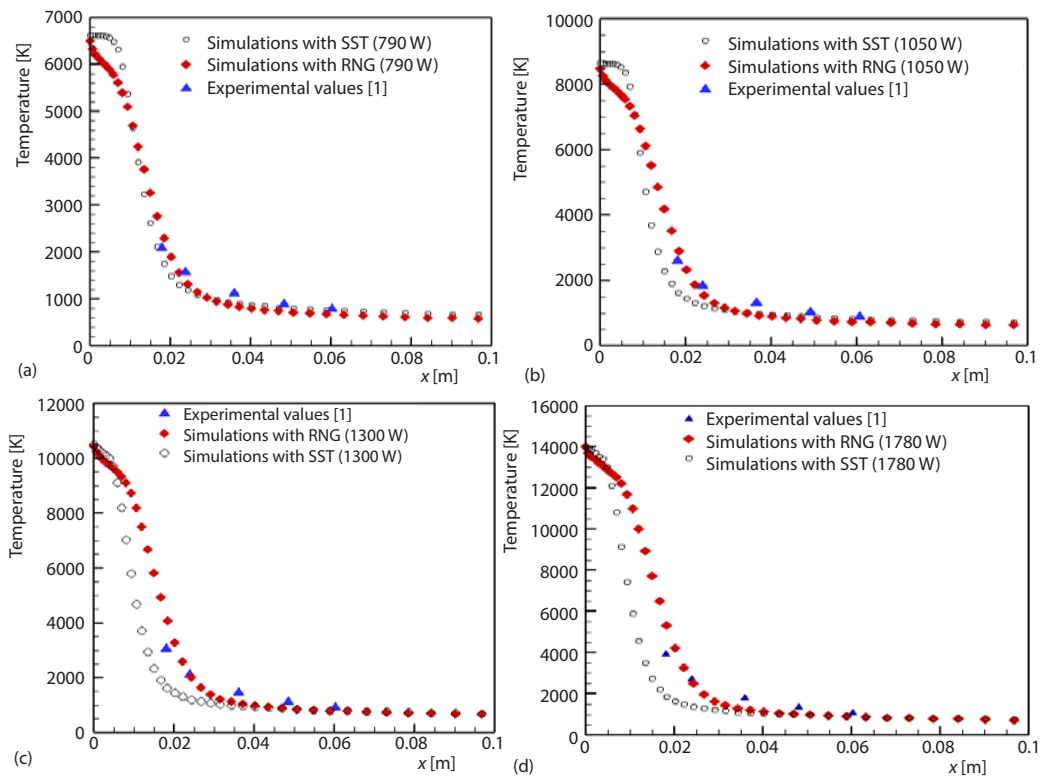


Figure 4. The 2-D thermal plasma jet temperature results for different values of power; (a) $P = 790$ W, (b) $P = 1050$ W, (c) $P = 1300$ W, and (d) $P = 1780$ W

jet model using CFX code will be presented comparing to experimental results, Snabre *et al.* [1] for different powers (790 W, 1050 W, 1300 W, and 1780 W). The temperature and velocity values at the nozzle exit are calculated from eqs. (6) and (8). The SST- $k-\omega$ and RNG $k-\epsilon$ turbulence models has been adopted to obtain simulations results. The comparison has been carried out between experimental and numerical simulations results. The results presented in figs. 4(a)-4(d) and figs. 5(a)-5(d) show the axial predicted temperature and velocity distributions of argon plasma jet for different values of power.

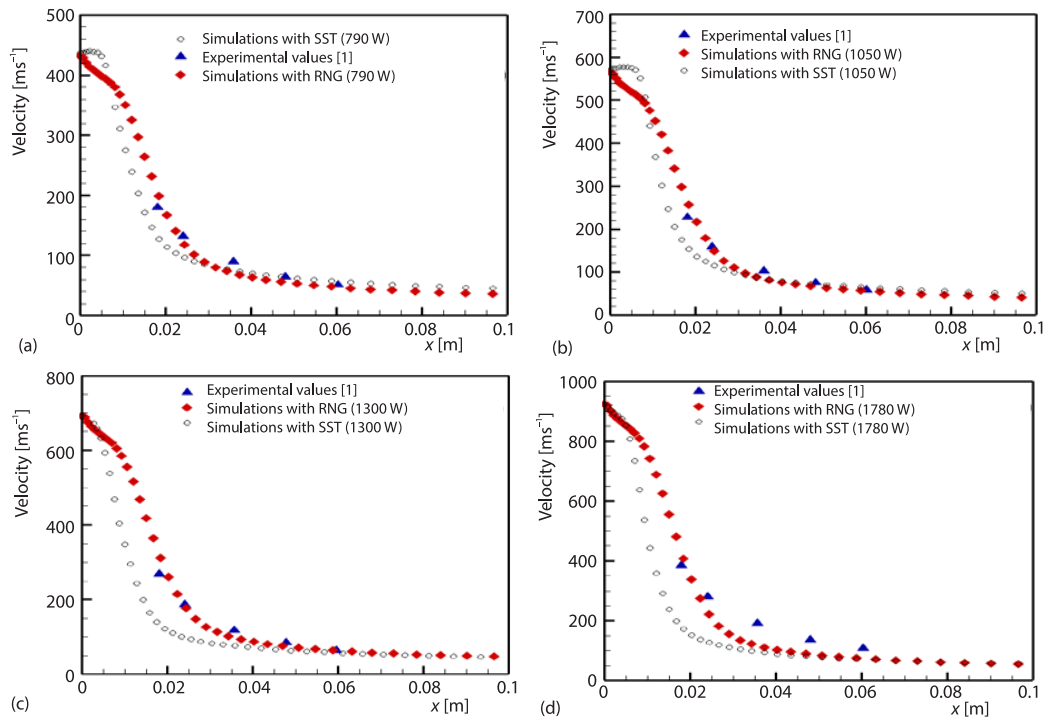


Figure 5. The 2-D thermal plasma velocity results for different values of power; (a) $P = 790$ W, (b) $P = 1050$ W, (c) $P = 1300$ W, and (d) $P = 1780$ W

It can be easily concluded that the results obtained (temperature and velocity distributions) by numerical simulations are very close to the experimental results for different values of power. For the CFX code, the velocity and temperature profiles calculated by using the RNG turbulence model are very close to experimental results, Snabre *et al.* [1], compared to the results obtained using the SST- $k-\omega$ model, the RNG turbulence model has given very accurate results compared to the experimental results. Note that in the range of 7-60 mm downstream of the nozzle exit x -axis, figs. 4(a)-4(d) and figs. 5(a)-5(d), the velocity and temperature decrease more rapidly for the SST model than for the RNG model, otherwise when x varies between 60 mm and 100 mm the velocity and temperature have widely the same values, figs. 4(a)-4(d) and figs. 5(a)-5(d). Figures 6(a) and 6(b) illustrate the variation of the axial temperature and velocity along the jet obtained by the RNG $k-\epsilon$ model for different effective power values, a nozzle diameter $d = 3$ mm and an argon flow $Q = 8.4$ Lpm. The predicted simulations results such as temperatures and velocities contours using ANSYS-CFX codes for different powers are shown in figs. 7(a)-7(c). In all cases, the stand-off distance is 100 mm but the velocity and temperature fields depends on the power of plasma jets. With this model of turbulence (RNG $k-\epsilon$), the

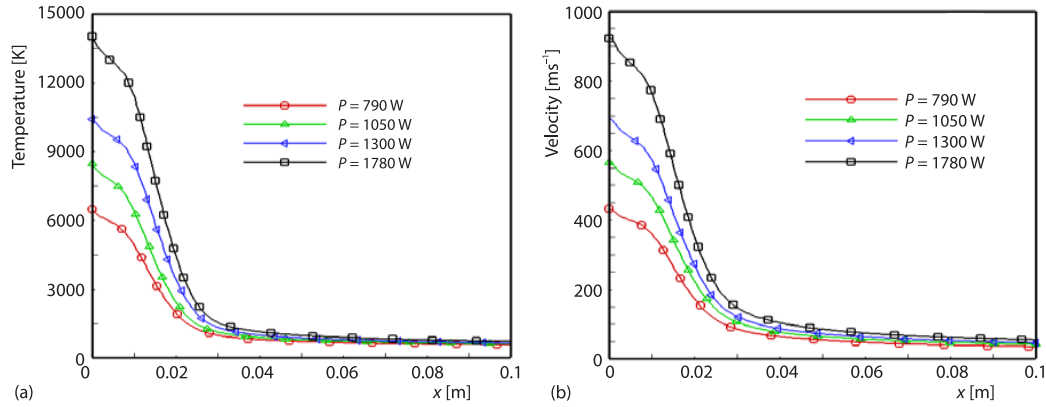


Figure 6. Distributions comparison for different powers; (a) for temperature and (b) for velocity

potential core of the plasma jet where the air has not yet penetrated extends a short distance downstream of the nozzle exit.

The analysis of figs. 5(a) and 5(b) and figs. 7(a)-7(c) indicates that the jet is composed of three regions: the first region ($x < 7$ mm) is the heart region defined by lines with a slight

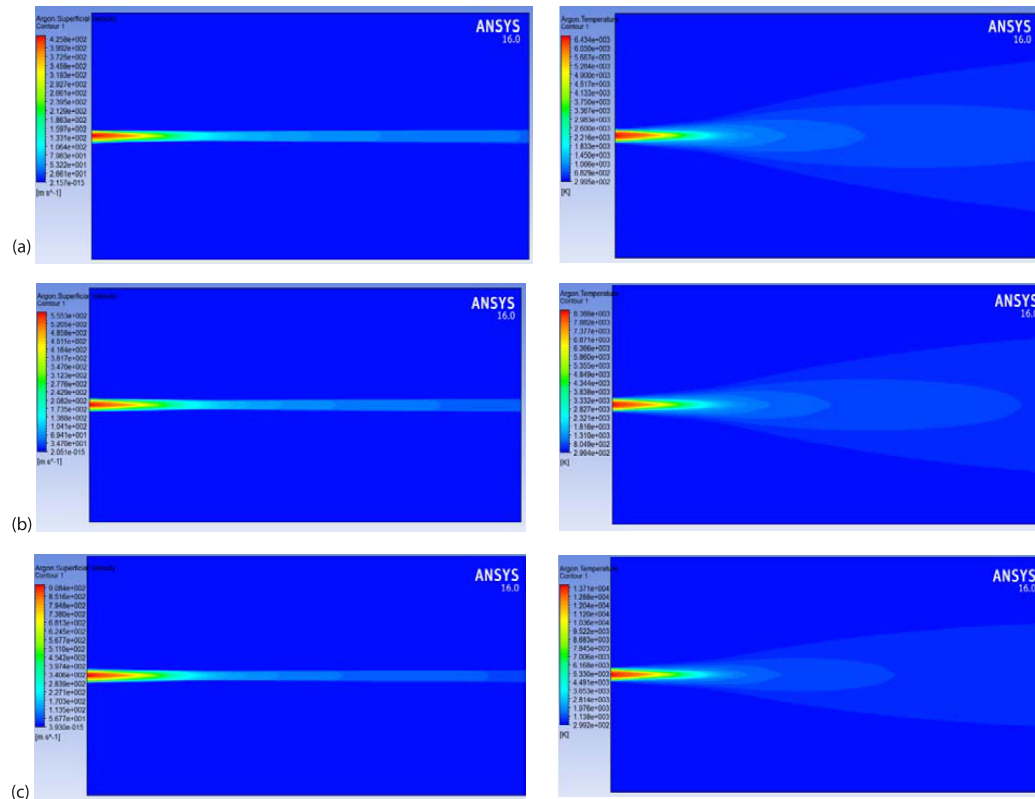


Figure 7. Velocity and temperature contours for different powers; (a) $P = 790$ W, (b) $P = 1050$ W, and (c) $P = 1780$ W

slope for temperature and velocities, the second is the developed region ($7 < x < 40$ mm) characterized by a quick decreasing in temperature and velocity profile along the jet and the third region ($40 < x < 100$ mm) is defined by a low gradient of velocity and temperature fields which gives almost constant values of these parameters.

For the Case b (when the effective power is 1050 W for example), a sudden decrease in velocity and temperature is very quickly observed after the position of 7 mm from the nozzle exit. This is due to the large-scale dissipation of the energy that results from entering the atmosphere. The ambient air absorbed by the jet cooled and slowed the flow. For this case (the effective power is 1050 W), velocity and temperature, which are initially 570 m/s and 8925 K at the nozzle exit, decrease considerably due to mixing with the cold and very dense ambient air to reach, respectively 41 m/s and 621 K at the end of the jet, fig. 7(c). The gradients of velocity and temperature are very high in the jet core. However, the introduction of the substrate in the calculation of the plasma jet flow requires a very high number of iterations to reach convergence for the steady-state simulations case. For this reason, unsteady-state is selected and the case of a 2-D thermal plasma spraying model is adopted by using CFX code with the same dimensions (100 mm and 50 mm for length and height, respectively). The nozzle diameter is 3.0 mm, and the computational domain dimensions for the substrate are 10 mm and 50 mm for length and height, respectively, and the substrate material is steel. The value of gas power used for these simulations is 1780 W.

The fig. 8 shows the argon temperature distributions along the axial line ($y = 25$ mm) of the plasma jet for different values of time and for $P = 1780$ W, it can be concluded that for $t > 60$ seconds the argon temperature distributions along the axial line are very close that it can be admitted that the convergence is reached. For $t = 6$ seconds, the argon temperature distribution is not uniform nor symmetrical this is due to the dissipation of the energy that results from cold ambient air, when $t > 60$ seconds the temperature distributions of argon converges to common distribution.

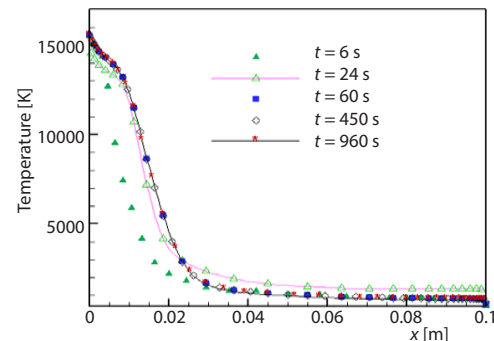


Figure 8. Argon temperature distributions for different values of time

To visualize the variation of the radial distributions of temperature and velocity according to the variation of time at various central positions (or different axial positions) the argon temperature and velocity profiles are presented in figs. 9(a)-9(d), this case is about an argon plasma jet discharging into the ambient air from a 3 mm nozzle of diameter under $P = 1780$ W with an argon flow rate of 8.4 Lpm.

It is noted that at $t = 6$ seconds the fraction of argon, fig. 10, keeps its maximum value of 100% for a distance of 10 mm downstream of the outlet of the nozzle, but at $t = 24$ seconds the fraction of argon keeps its maximum value of 100% for a distance of 40 mm which means that the plasma jet core, where the air has not still penetrated, extends 10 and 40 mm, respectively downstream of the nozzle exit. The decay then occurs very rapidly as soon as the transition turbulence occurs (increase in the diffusion of heat, momentum and species). Plasma gas mixes with ambient air as a result of species diffusion and the mass fraction of air reaches 100% at the end of the domain for all values of time.

Furthermore, the temperature distribution of the substrate for five values of time at the stand-off distance of 100 mm and for a gas power $P = 1780$ W are shown in figs. 11(a)-11(e).

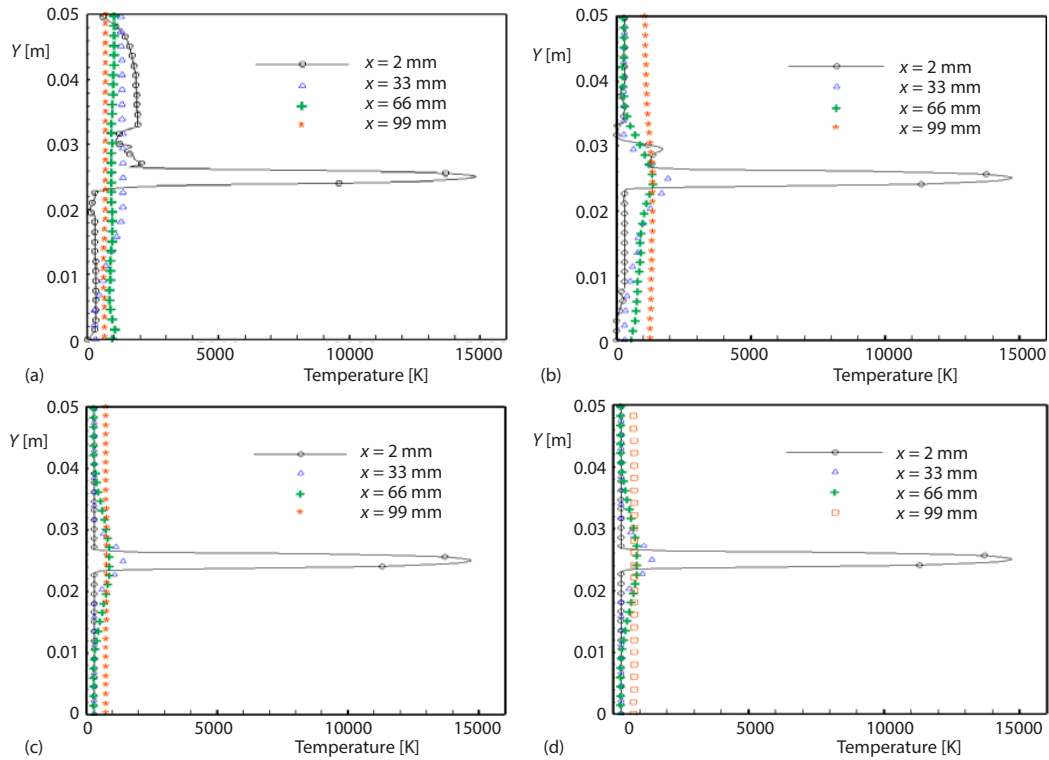


Figure 9. Argon temperature profiles at different axial positions at different times; (a) $t = 6$ seconds, (b) $t = 24$ seconds, (c) $t = 60$ seconds, and (d) $t = 450$ seconds

For all values of time, temperature decreases along the x -axis and y -axis of the substrate and the maximal of temperature is located in the centre of the substrate at the stand-off distance of 100 mm. The heat radial diffusion of the substrate influences the temperature profiles in the substrate for values of x from 100-110 mm, these profiles are symmetrical but they are not linear.

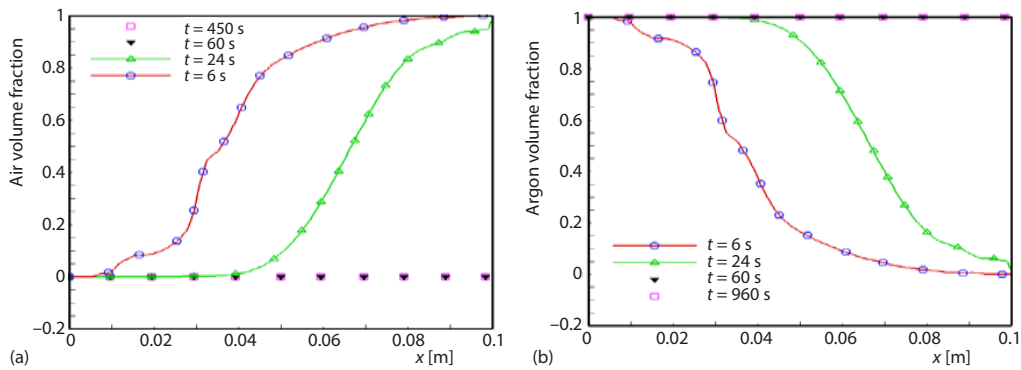


Figure 10. Volume fraction along centerline plasma jet; (a) for air and (b) for argon

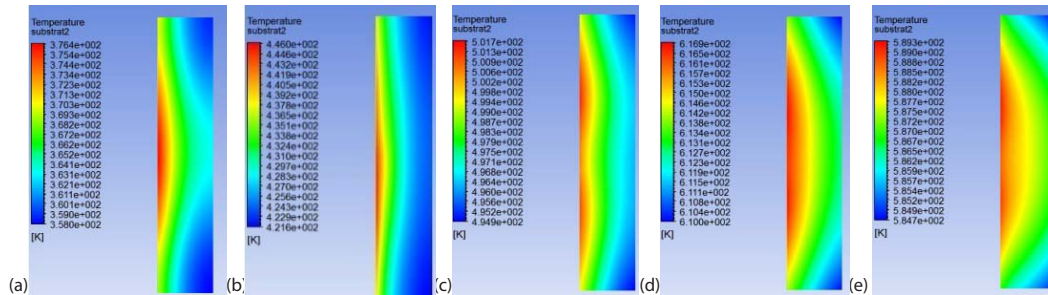


Figure 11. Predicted temperature distribution of the substrate for five values of time;
 (a) $t = 6$ seconds, (b) $t = 24$ seconds, (c) $t = 60$ seconds, (d) $t = 450$ seconds, and (e) $t = 960$ seconds

Conclusion

In this paper a 2-D thermal plasma jet has been simulated by using the ANSYS-CFX code with two models of turbulence for different cases of effective powers. The analysis of turbulent flow during thermal jet using the RNG- $k-\epsilon$ and the SST- $k-\omega$ models was also presented. Both velocity and temperature profiles at the nozzle exit have been calculated and used as inlet boundaries conditions. The results obtained from the two models of turbulence show that the RNG- $k-\epsilon$ model with different effective powers (790 W, 1050 W, 1350 W, and 1780 W) are in better agreement with the experimental results. The RNG- $k-\epsilon$ model gave results closer to the experimental than the results obtained from the SST- $k-\omega$ model. It can also be concluded that when increasing the power supplied to the gas used, the temperature increases and it is maximum in the centraline. In the second step, the flow analyzed by the RNG- $k-\epsilon$ model has generated the initial conditions for the unsteady flow. The transient simulations for plasma jet are done to carry out the velocity and temperature fields and also to obtain the substrate temperature distribution for different values of time. The results obtained show that the variation of the temperature of the plasma jet is insignificant near to the substrate for any value of time for the case of the transient regime.

Nomenclature

c_p	– specific heat capacity at constant pressure, [kJkg ⁻¹ K ⁻¹]	v	– y -velocity, [ms ⁻¹]
D	– mass diffusion coefficient, [m ² s ⁻¹]	w	– w -velocity [ms ⁻¹]
k	– kinetic energy due to turbulence, [m ² s ⁻²]	y	– masse fraction of the species, [–]
P	– power, [W]	<i>Greek symbols</i>	
Pr_t	– turbulent Prandtl number, [–]	λ	– thermal conductivity [Wm ⁻¹ K ⁻¹]
p	– pressure, [bar]	μ_{eff}	– effective viscosity [m ² s ⁻¹]
q_{cond}	– conductive heat flux, [Wm ⁻²]	μ_t	– turbulent viscosity [m ² s ⁻¹]
q_{conv}	– convective heat flux, [Wm ⁻²]	ϕ	– dependent variable, [–]
u	– x -velocity, [ms ⁻¹]		

References

- [1] Snabre, P., et al., Heat Transfer around a Spherical Particle Levitated in Argon Plasma Jet, *The Euro. Physical Journal Applied Physics*, 3 (1998), 3, pp. 287-293
- [2] Fauchais, P. L., et al., *Thermal Spray Fundamentals*, Springer, Boston, Mass., USA, 2014
- [3] Zhao, Y., et al., Influence of Substrate Properties on the Formation of Suspension Plasma Sprayed Coatings, *Journal Therm. Spray Technol.*, 27 (1997), 8, pp. 73-83
- [4] Huang, P. C., et al., A Two-Fluid Model of Turbulence for a Thermal Plasma Jet, *Plasma Chemistry and Plasma Processing*, 15 (1995), Mar., pp. 25-46

- [5] Chen, C. Z., et al., Improved Hardness and Corrosion Resistance of Iron by Ti/TiN Multilayer Coating and Plasma Nitriding Duplex Treatment, *Surface & Coatings Technology*, 204 (2010), 18-19, pp. 3082-3086
- [6] Bolot, R., et al., On the Use of a Low-Reynolds Extension the Chen Kim $k-\epsilon$ Model to Predict Thermal Exchanges in the Case of an Impinging Plasma Jet, *International Journal of Heat and Mass Transfer*, 44 (2001), 6, pp. 1095-1106
- [7] Qunbo, F., et al., Modelling Influence of Basic Operation Parameters on Plasma Jet, *Journal of Materials Processing Techn.*, 198 (2008), 1-3, pp. 207-212
- [8] Abdellah El-hadj, A., Ait Messaoudene, N., Comparison between Two Turbulence Models and Analysis of the Effect of the Substrate Movement on the Flow Field of a Plasma Jet, *Plasma Chem. and Plasma Processing*, 25 (2005), Dec., pp. 699-722
- [9] Selezneva, S. E., Boulos, M. I., Supersonic Induction Plasma Jet Modelling, *Nuclear Instruments and Methods in Physics Research*, B180 (2001), 1-4, pp. 306-311
- [10] Zhang, T., et al., Effect of a Moving Flame on the Temperature of Polymer Coatings and Substrates, *Progress in Organic Coatings*, 70 (2011), 1, pp. 45-51
- [11] Murphy, A. B., Arundell, C. J., Transport Coefficients of Argon, Nitrogen, Oxygen, Argon-Nitrogen, and Argon-Oxygen Plasmas, *Plasma Chemistry and Plasma Processing*, 14 (1994), Dec., pp. 451-490
- [12] Murphy, A. B., Transport Coefficients of Air, Argon-Air, Nitrogen-Air, and Oxygen-Air Plasmas, *Plasma Chemistry and Plasma Processing*, 15 (1995), June, pp. 279-307
- [13] Selvan, B., et al., Modelling of the Plasma-Substrate Interaction and Prediction of Substrate Temperature during the Plasma Heating, *Eur. Phys. J. D*, 61 (2011), 3, pp. 663-675
- [14] Chen, X., Li, H. P., 3-D flow and Heat Transfer in Thermal Plasma Systems, *Surface and Coatings Technology*, 171 (2003), 1-3, pp. 124-133
- [15] Qunbo, F., et al., 3-D Simulation of the Plasma Jet in Thermal Plasma Spraying, *Journal of Materials Processing Technology*, 166 (2005), 2, pp. 224-229
- [16] Bolot, R., et al., Mathematical Modelling of a Plasma Jet Impinging on Flat Structure, *Proceedings*, 15th International Thermal Spray Conference, Nice, France, 1998
- [17] Hugo, F., et al., Modelling of a substrate thermomechanical behavior during plasma- spraying, *Journal of Materials Processing Technology*, 190 (2007), 1-3, pp. 224-229.
- [18] Gonzalez, J. J., et al., Comparisons between Two-and 3-D Models, Gas Injection and Arc Attachment, *Journal Phys. D. Appl. Phys.*, 35 (2002), 24, pp. 3181-3191
- [19] Selvan, B., et al., The 3-D Numerical Modelling of an Ar-N₂ Plasma Arc Inside a Non-Transferred Torch, *Plasma Science and Technology*, 11 (2009), 6, 679
- [20] Mariaux, G., Vardelle, A., 3-D Time-Dependent Modelling of the Plasma Spray Process – Part 1: Flow Modelling, *International Journal of Thermal Science*, 44 (2005), 4, pp. 357-366
- [21] Marchand, C., et al., Liquid Precursor Plasma Spraying: Modelling the Interactions between the Transient Plasma Jet and the Droplets, *Journal of Thermal Spray Technology*, 16 (2007), Oct., pp. 705-712
- [22] ANSYS FLUENT 6.3.26 User's Guide and Update Manual, Fluent, Inc., 10 Cavendish Court, Lebanon, NH 03766, 1995-2009
- [23] Pateyron, B., et al., Thermodynamic and Transport Properties of Ar-H₂ and Ar-He Plasma Gases Used for Spraying at Atmospheric Pressure I: Properties of the Mixtures, *Plasma Chem. and Plasma Process.*, 12 (1992), Dec., pp. 421-448